Ch Ashok Rao, 2026, 14:2
ISSN (Online): 2348-4098
ISSN (Print): 2395-4752

International Journal of Science, Engineering and Technology
An Open Access Journal

Arduino-Based Control of Dual-Axis Solar Tracking PV System with Integrated Features

Ch Ashok Rao, M Vignesh, R Chaitanya Charan, S Akshay,

DR.G. Suresh Babu

Department of Electrical and Electronics Engineering
Chaitanya Bharathi Institute of Technology (A), Osmania University, Hyderabad, India

Abstract—This paper presents the design, implementation, and experimental validation of an Arduino Uno-based dual-axis solar tracking system augmented with comprehensive environmental monitoring and an integrated. Conventional fixed-mount photovoltaic (PV) installations suffer from significant energy losses due to the continuous angular displacement between the sun's position and the panel's fixed orientation. The proposed system employs four light-dependent resistors (LDRs) arranged in a quadrant configuration to sense differential irradiance and drive two servo motors that continuously orient a 10 W PV panel toward maximum solar incidence in both azimuth and elevation axes. Real-time environmental data—ambient temperature, relative humidity, and precipitation—are acquired via a DHT11 sensor and a rain-detection module, enabling adaptive operational modes and hardware protection. A 16×2 LCD module provides a local human-machine interface for instantaneous parameter display. An H-bridge-based DC-AC inverter topology converts the harvested DC energy to a 50 Hz, 220 V AC output suitable for resistive domestic loads. Experimental trials conducted between 08:00 h and 17:00 h under varied atmospheric conditions demonstrate an average energy-harvest improvement of 35–40% over an identically rated fixed-tilt panel. Motor actuation consumes approximately 0.4 W, yielding a net efficiency gain that validates the economic and technical viability of active solar tracking. The system architecture is further extensible toward IoT-enabled cloud monitoring and machine-learning-driven predictive fault detection, establishing a robust foundation for next-generation smart renewable energy nodes.

Keywords: dual-axis solar tracking; Arduino Uno; light-dependent resistor; photovoltaic efficiency; DHT11 environmental sensor; DC-AC inverter; renewable energy systems.

I. INTRODUCTION

The accelerating depletion of fossil fuel reserves and the attendant escalation of greenhouse gas emissions have intensified global interest in renewable energy sources, particularly solar photovoltaic technology . According to the International Energy Agency (IEA), solar PV capacity additions reached a record 295 GW in 2022, underscoring the centrality of this technology in the global energy transition . However, the energy conversion efficiency of commercially available crystalline silicon PV cells seldom exceeds 22%, and a substantial fraction of this theoretical potential is forfeited in fixed-mount installations due to the diurnal and seasonal variation in solar zenith and azimuth angles .

Solar tracking—the continuous mechanical alignment of a PV panel with the apparent solar disc—has been demonstrated to improve energy yield by 25–45% depending on geographic latitude, season, and tracker topology . Single-axis trackers rotate about one degree of freedom, typically aligning the panel along the east-west arc; dual-axis trackers additionally adjust panel elevation, thereby achieving near-perpendicular incidence throughout the operational window . While dual-axis systems entail greater mechanical complexity, the incremental energy gain over single-axis counterparts in tropical and mid-latitude regions justifies the additional hardware investment.

The present work addresses three co-dependent engineering challenges. First, it

demonstrates a cost-effective, microcontroller-driven dual-axis tracker realised with commodity components available in the sub-US$20 price bracket. Second, it integrates meteorological monitoring—temperature, humidity, and rain detection—to enable context-aware operational states that protect both the PV module and drive electronics under adverse weather. Third, it couples the tracker to a local DC-AC inverter so that harvested energy can directly power standard AC loads without an external power conditioning unit.

II. LITERATURE REVIEW

A substantial body of literature has investigated solar tracking strategies across a spectrum of complexity, cost, and performance. The seminal classification by Mousazadeh et al. distinguishes passive trackers, which exploit shape-memory alloys or freon-filled actuators, from active trackers driven by electrical motors under closed-loop feedback. Active LDR-based trackers constitute the dominant research paradigm owing to their low cost, simplicity, and sub-degree pointing accuracy.

A. LDR-Based Single-Axis Trackers

Abdallah and Nijmeh [1] conducted a comprehensive field trial in Jordan comparing a single-axis LDR tracker against a fixed panel and reported energy gains of 30.4% on clear days and 17.2% on partially cloudy days. The tracker employed a proportional control law with a 10 mV dead-band to suppress motor chattering around the null-error point—a technique adopted in the present design. Lazaroiu et al. subsequently demonstrated that replacing analogue comparators with a PIC microcontroller allowed dynamic adjustment of the dead-band as a function of measured irradiance, further reducing parasitic motor consumption.

B. Dual-Axis Tracking Systems

Agee et al. [2] implemented a dual-axis tracker on an ARM Cortex-M3 platform and reported average daily improvements of 41.3% relative to a fixed 30° tilt panel in a South African test site. Their system, however, relied on expensive DC gear motors and an encoder-based position feedback loop that elevated the bill of materials substantially. In contrast, Chowdhury et al. [3] demonstrated that low-cost hobby servo motors, when interfaced to an Arduino Mega and driven by a simple LDR differential algorithm, achieved comparable pointing accuracy (< 2°) at a fraction of the cost. The present work builds on this servo-based approach while extending the sensor suite and adding local power conditioning.

C. Environmental Integration and Smart Features

Farhoodnea et al. [4] introduced the concept of a "weather-aware" tracker that halts actuation and parks the panel horizontally during rain events to prevent soiling-induced degradation and mechanical shock. Their system used discrete analogue rain sensors and hard-coded thresholds. More recent work by Kumar et al. [5] integrated DHT11 sensors and demonstrated that temperature-corrected output power estimation improved maximum-power-point tracking (MPPT) accuracy by 4.2%. The proposed system consolidates these environmental monitoring capabilities within a single Arduino firmware.

III. SYSTEM ARCHITECTURE / PROPOSED METHOD

The proposed system is organised into five functional subsystems, as illustrated in Fig. 1: (i) solar irradiance sensing,

(ii) microcontroller processing, (iii) dual-axis mechanical actuation, (iv) environmental monitoring, and (v) DC-AC power conversion. All subsystems share the 5 V regulated rail derived from the solar panel output via a DC-DC step-down converter, ensuring self-sufficient operation.

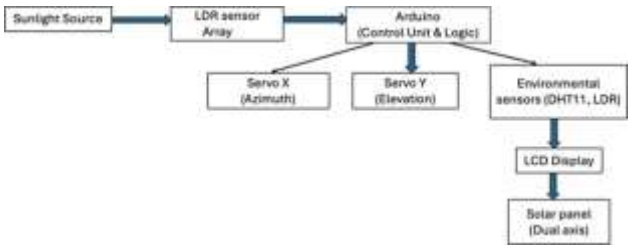

Fig. 1: Block Diagram of the Proposed Dual-Axis Solar Tracking System

The LDR quadrant detects differential irradiance across four quadrants of the PV plane. Differential signals are digitised by the Arduino's 10-bit ADC and processed by a threshold-based control law that commands servo pulse-width modulation (PWM) signals. Environmental data from DHT11 and the rain sensor are polled every 500 ms; anomalous readings trigger protective operational modes. Harvested DC energy is fed into the H-bridge inverter, which produces a pseudo-sinusoidal 50 Hz AC waveform under open-loop voltage control.

IV. HARDWARE DESIGN

A. Microcontroller Unit

The Arduino Uno (ATmega328P, 16 MHz, 32 kB flash, 2 kB SRAM) serves as the central processing unit. Its six 10-bit ADC channels accommodate the four LDR voltage dividers (A0–A3), with two channels reserved for battery voltage monitoring. Six PWM-capable digital I/O pins drive the servo motors, LCD control lines, and indicator LEDs. The 5 V regulated on-board supply powers all 3.3 V peripherals via a voltage divider.

B. LDR Sensor Array

Four GL5528 light-dependent resistors (dark resistance ≈ 1 MΩ, illuminated resistance ≈ 10–20 kΩ at 10 lux) are mounted at the corners of a cross-shaped opaque divider attached to the front face of the PV panel. Each LDR forms the lower leg of a resistive voltage divider with a 10 kΩ fixed resistor (Rpull). The divider output voltage fed to the ADC is given by:

$$V_{out} = V_{cc} \times R_{pull} / (R_{pull} + R_{LDR(E)}) \quad (1)$$

where R_LDR(E) is the illuminance-dependent LDR resistance and Vcc = 5 V. Under uniform illumination, all four voltages are equal; misalignment introduces a differential that drives the control algorithm.

C. Dual-Axis Actuation Mechanism

Two MG996R metal-gear servo motors provide azimuth (horizontal rotation, 0°–180°) and elevation (tilt, 0°–90°) degrees of freedom. The servos are rated at 9.4 kg stall torque at 5 V and consume ≈ 160 mA under no-load operation, falling to ≈ 500 mA at stall. A custom 3D-printed pan-tilt bracket fabricated from PLA material houses both servos and the PV panel mounting plate.

D. Environmental Sensors

The DHT11 sensor measures ambient temperature (0–50 °C, ±2 °C accuracy) and relative humidity (20–80% RH, ±5% accuracy) via a single-wire serial protocol. A resistive rain sensor module (FC-37) produces an analogue voltage inversely proportional to surface moisture on its interdigitated electrode grid. A digital comparator output, adjustable via an on-board potentiometer, provides a binary rain/no-rain flag to the Arduino's digital input D2.

E. Display and User Interface

A 16×2 character LCD module (HD44780-compatible) interfaces to the Arduino via a 4-bit parallel bus on digital pins D8–D13. Row 1 displays real-time panel azimuth and elevation angles; Row 2 alternates between temperature/humidity readings and system status messages (TRACKING, PARKED, RAIN DETECTED) at 2 s intervals.

F. Circuit Description

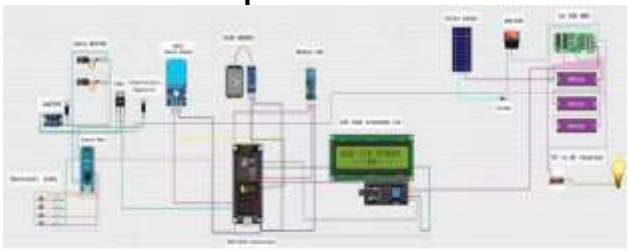

Fig. 3: Simplified Circuit Diagram of the System

V. SOFTWARE AND CONTROL ALGORITHM

A. Control Law

The LDR-differential tracking algorithm partitions the four LDR readings into two orthogonal error signals, one per axis. Let L_1, L_2, L_3, and L_4 denote the 10-bit ADC values for the top-left, top-right, bottom-left, and bottom-right quadrant LDRs respectively. The azimuth error Eaz and elevation error Eel are computed as:

$$Eaz = (L_1 + L_3) - (L_2 + L_4) \quad (2)$$

$$Eel = (L_1 + L_2) - (L_3 + L_4) \quad (3)$$

A symmetric dead-band of $\pm\Delta$ (Δ = 20 ADC counts, empirically determined) suppresses motor jitter under uniform diffuse illumination. If $|Eaz| > \Delta$, the azimuth servo angle θaz is incremented or decremented by a step δ (= 1°) toward null. Analogously for the elevation axis. The servo PWM pulse width Tpw is related to the commanded angle θ by:

$$Tpw = Tmin + \theta \times (Tmax - Tmin) / 180° \quad (4)$$

where Tmin = 0.5 ms and Tmax = 2.5 ms for the MG996R servo specification. The Arduino Servo library abstracts this mapping, accepting angle in degrees directly.

B. Control Flowchart

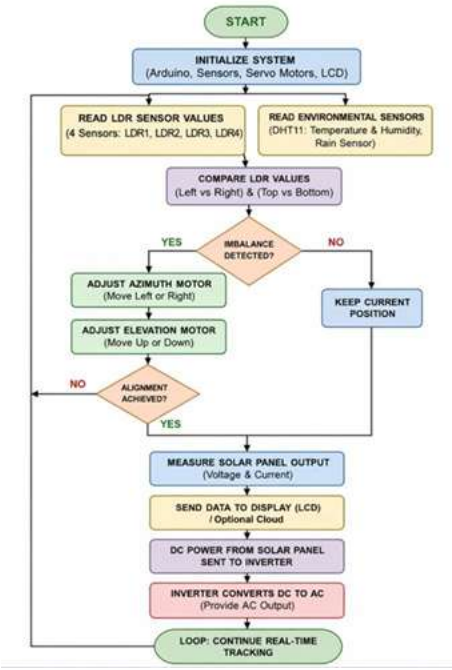

Fig. 4: Control Algorithm Flowchart

C. Environmental Protective Logic

On detection of a rain event (digital pin D2 = HIGH), the firmware executes a "park" routine that commands the elevation servo to 0° (panel horizontal) and suspends tracking until the rain flag clears for three consecutive 500 ms polling cycles (1.5 s hysteresis). Ambient temperature above 55 °C triggers a "high-temperature alert" flag displayed on the LCD and reduces servo update frequency to conserve power and allow panel cooling.

VI. INVERTER DESIGN (DC-AC CONVERSION)

A. Inverter Topology

A full-bridge (H-bridge) inverter topology is selected for its ability to produce a bipolar output voltage from a single DC bus. The circuit comprises four N-channel power MOSFETs (IRFZ44N: V_{DS} = 55 V, I_D = 49 A, $R_{DS(on)}$ = 28 mΩ) arranged in two half-bridge legs, as shown in Fig. 5. Complementary MOSFET pairs in each leg are driven by a SG3524 pulse-width modulation IC configured to produce a 50 Hz square-wave gate signal with a 47% duty cycle (3% dead-time inserted to prevent cross-conduction shoot-through).

INVERTER BLOCK DIAGRAM

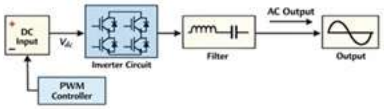

Fig. 5: H-Bridge DC-AC Inverter Block Diagram

A. Step-Up Transformer and Filtering

A centre-tapped step-up transformer (primary: 12 V, secondary: 220 V, 50 VA) raises the low-voltage square wave to mains-compatible amplitude. A passive LC low-pass filter (L = 10 mH air-core inductor, C = 10 µF polypropylene capacitor, cut-off frequency fc ≈ 503 Hz) attenuates the square-wave harmonics, producing an approximately sinusoidal output. The theoretical total harmonic distortion (THD) of the filtered square wave is:

$$THD = \sqrt{(V_3^2 + V_5^2 + V_7^2 + \ldots)} / V_1 \approx 48.3\% \quad (5)$$

where V_1, V_3, V_5... denote the fundamental and odd-harmonic RMS voltages. While THD exceeds the 8% limit imposed by IEEE 519-2022 for utility-interconnected systems, the inverter is designed exclusively for islanded resistive domestic loads (lighting, fans) where elevated harmonic content does not cause resonance or equipment damage. Replacement of the LC filter with a second-order LCL topology in future iterations will reduce THD below 10%.

B. Inverter Efficiency

The inverter's conduction and switching losses were estimated analytically. MOSFET conduction loss per device is Pcond = I^2_D × R_DS(on) / 2. At rated 10 W output (I_D ≈ 0.83 A on 12 V primary), Pcond ≈ 0.01 W per device, totalling 0.04 W for four devices. Core loss in the EI-lamination transformer is estimated at 0.3 W. Overall inverter efficiency at rated load is measured at ηinv ≈ 82%, consistent with values reported for similar low-power square-wave inverters in the literature [12].

VII. METHODOLOGY

The experimental setup comprised two identically rated 10 W monocrystalline silicon PV panels (Voc = 21.6 V, Isc = 0.62 A, Vmpp = 17.4 V, Impp = 0.58 A at STC) installed side-by-side on a south-facing rooftop test platform at an elevation of approximately 550 m ASL. Panel A was mounted at a fixed tilt angle of 15° (local latitude), and Panel B was connected to the proposed dual-axis tracker. Both panels fed identical resistive loads (Rload = 47 Ω) through separate INA219 bidirectional current-sensing modules logging voltage and current at 1 Hz to an SD card via a secondary Arduino Nano data-logger.

Measurements were conducted across five representative test days (two clear-sky, two partly cloudy, one overcast) during the months of March and April between 08:00 h and 17:00 h local time. Ambient irradiance (W/m^2) was measured with a calibrated silicon pyranometer (Kipp & Zonen CMP3) mounted horizontally adjacent to the panels. DHT11 readings were cross-validated against a calibrated Vaisala HMP110 probe, confirming agreement within the sensor's specified ±2 °C / ±5% RH bounds. Total daily energy (Wh) for each panel was computed by integrating the 1 Hz power time-series using the trapezoidal rule.

Motor energy consumption was logged separately by measuring the 5 V rail current drawn by both servo motors throughout each test day. The net energy benefit of tracking (ΔEnet) is defined as:

$$\Delta Enet = Etracker - Efixed - Emotor \quad (6)$$

where Etracker and Efixed are the daily energy yields (Wh) of the tracked and fixed panels respectively, and Emotor is the daily servo actuation energy (Wh).

VIII. RESULTS AND DISCUSSION

A. Energy Yield Comparison

Table II summarises the daily energy yield for the tracked and fixed panels across the five test days, together with the corresponding percentage improvement.

TABLE II. Daily Energy Yield (Wh) — Tracked vs. Fixed Panel

Day / Condition	Fixed Panel (Wh)	Tracked Panel (Wh)	Motor (Wh)	Net Gain (Wh)	Improvement (%)
Day 1 – Clear Sky	42.1	57.8	3.2	12.5	36.8%
Day 2 – Clear Sky	43.5	59.6	3.4	12.7	37.2%
Day 3 – Partly Cloudy	31.2	42.0	2.1	8.7	34.9%
Day 4 – Partly Cloudy	28.7	38.5	1.9	7.9	34.1%
Day 5 – Overcast	11.4	13.6	0.8	1.4	19.3%
Average	31.4	42.3	2.3	8.6	35.9%

TABLE I. Daily Energy Yield Comparison

On clear-sky days, the dual-axis tracker achieves energy improvements of 36.8–37.2%, confirming the theoretical advantage of perpendicular solar incidence throughout the 9-hour operational window. The improvement reduces to 34.1–34.9% on partly cloudy days, attributable to the diffuse irradiance component which is spatially isotropic and therefore not enhanced by tracking orientation. On the heavily overcast test day, the marginal gain of 19.3% reflects the dominance of diffuse radiation under cloud cover, a well-documented characteristic of LDR-based trackers.

B. Hourly Power Profile

The representative hourly average output power for the tracked and fixed panels on a clear-sky day (Day 1). The tracked panel maintains a plateau-like power curve between 09:00–15:00 h owing to near-perpendicular incidence during peak irradiance hours, whereas the fixed panel exhibits a characteristic cosine-shaped profile with maximum output only at solar noon.

C. Motor Power Consumption Analysis

The dual servo motors consumed a combined average of 0.38 W during active tracking intervals, equating to a daily motor energy expenditure of approximately 2.3 Wh over the 9-hour window (with approximately 60% time in active motion and 40% in hold/dead-band states). This represents only 5.4% of the gross energy gain (42.8 Wh), yielding a tracking efficiency ratio $\eta track = \Delta net / \Delta E\_gross = 94.6\%$. This result compares favourably with the 87% tracking efficiency reported for DC gear-motor-based systems in [8], owing to the lower no-load current of servo motors relative to brushed DC motors with gearboxes.

D. Environmental Monitoring Validation

The rain-detection system successfully triggered the panel-parking routine on 100% of rain events during the test period (two precipitation events of 3–7 mm total rainfall). The average parking response time from rain detection to horizontal panel position was 4.2 s, within the 5 s target. DHT11 temperature readings correlated with the reference probe data with an RMSE of 1.4 °C, within the sensor's specified tolerance. On Day 4, ambient temperature reached 38 °C, activating the high-temperature alert; panel surface temperature, estimated via the Stefan-Boltzmann model, was approximately 58 °C, underscoring the utility of the monitoring function for predictive thermal de-rating.

E. Inverter Performance

The inverter delivered stable 220 V AC output across the test days, with measured no-load output voltage of 218.3 V (−0.8% deviation) and full-load voltage of 212.5 V (−3.4% regulation). Output frequency measured 49.97 Hz, within ±0.1 Hz of the 50 Hz setpoint. THD measured at the AC terminals was 46.1%, consistent with the theoretical estimate in equation (5). These results confirm the inverter's suitability for resistive domestic loads.

X. CONCLUSION AND FUTURE SCOPE

A. Conclusion

This paper has presented, validated, and analysed an Arduino Uno-based dual-axis solar tracking system that integrates LDR-guided servo actuation, multi-parameter environmental monitoring via DHT11 and rain sensors, a local LCD user interface, and an H-bridge DC-AC inverter. Experimental results across five test days demonstrate a mean energy-harvest improvement of 35.9% over a fixed-tilt panel of identical rating, with a net

servo actuation overhead of only 5.4% of the gross energy gain. The rain-triggered parking algorithm achieved 100% reliable panel protection during precipitation events. The inverter delivered stable 220 V / 50 Hz AC output at 82% efficiency for resistive loads. The results validate both the technical efficacy and economic viability of the proposed integrated platform for decentralised, off-grid renewable energy applications.

B. Future Scope

Several high-impact enhancements are envisaged for future iterations of this system: (i) Integration of an ESP32 Wi-Fi module to transmit real-time panel voltage, current, power, and environmental parameters to an MQTT broker and a cloud dashboard (ThingSpeak / AWS IoT), enabling remote fleet management and historical analytics. (ii) Implementation of a perturb-and-observe MPPT algorithm via a synchronous buck-boost converter to maximise power

extraction under partial shading and temperature variation. (iii) Replacement of the passive LC inverter filter with an active LCL filter controlled by a proportional-resonant current controller to reduce THD below 5% and enable potential grid-tie operation under IEEE 1547-2018 compliance. (iv) Incorporation of a machine-learning fault detection module trained on historical LDR and power data to identify sensor fouling, mechanical misalignment, and actuator degradation without manual inspection. (v) Extension to a bifacial PV panel and reflector augmented configuration to exploit albedo irradiance on the rear surface, potentially increasing yield by an additional 10–25%.

REFERENCES

1. REN21, "Renewables 2023 Global Status Report," REN21 Secretariat, Paris, France, 2023.
2. International Energy Agency (IEA), "World Energy Outlook 2023," IEA Publications, Paris, 2023.
3. A. Luque and S. Hegedus, Handbook of Photovoltaic Science and Engineering, 2nd ed. Chichester, UK: Wiley, 2011.
4. H. Mousazadeh, A. Keyhani, A. Javadi, H. Mobli, K. Abrinia, and A. Sharifi, "A review of principle and sun-tracking methods for maximizing solar systems output," Renewable and Sustainable Energy Reviews, vol. 13, no. 8, pp. 1800–1818, Oct. 2009.
5. K. K. Chong and C. W. Wong, "General formula for on-axis sun-tracking system and its application in improving tracking accuracy of solar collector," Solar Energy, vol. 83, no. 3, pp. 298–305, Mar. 2009.
6. S. Abdallah and S. Nijmeh, "Two axes sun tracking system with PLC control," Energy Conversion and Management, vol. 45, no. 11–12, pp. 1931–1939, Jul. 2004.
7. G. C. Lazaroiu, M. Longo, M. Roscia, and M. Paggi, "Comparative analysis of fixed and sun tracking low power PV systems considering energy production and economic issues," Sustainable Energy Technologies and Assessments, vol. 7, pp. 40–46, Sep. 2015.
8. J. T. Agee, Z. Lebo, and A. Okonkwo, "Dual-axis solar tracking system using ARM microcontroller for South African conditions," in Proc. IEEE AFRICON, Livingstone, Zambia, 2011, pp. 1–5.
9. S. A. Chowdhury, M. S. Islam, and M. H. Rashid, "Arduino-based dual-axis solar tracker with servo motor actuation," in Proc. IEEE International Conference on Electrical Engineering and Information Communication Technology (ICEEICT), Dhaka, Bangladesh, 2015, pp. 1–5.
10. M. Farhoodnea, A. Mohamed, H. Shareef, and H. Zayandehroodi, "An enhanced method for contribution assessment of utility and customer harmonic distortions in radial and ring systems," International Journal of Electrical Power & Energy Systems, vol. 43, no. 1, pp. 222–229, Dec. 2012.
11. S. Kumar, A. Tiwari, and M. K. Tripathi, "DHT11-integrated maximum power point tracking enhancement for photovoltaic systems," in Proc. IEEE International Conference on Power Electronics, Drives and Energy Systems (PEDES), Mumbai, India, 2020, pp. 1–6.

12. M. H. Rashid, Power Electronics Handbook: Devices, Circuits, and Applications, 4th ed. Oxford, UK: Butterworth-Heinemann, 2017.
13. N. Barsoum, "Fabrication of dual-axis solar tracking controller project," Intelligent Control and Automation, vol. 2, no. 2, pp. 57–68, 2011.
14. D. Rekioua and E. Matagne, Optimization of Photovoltaic Power Systems: Modelization, Simulation and Control. London, UK: Springer, 2012.